

Physics of the Edwards-Anderson Spin Glass in Dimensions $d = 3, \dots, 8$ from Heuristic Ground State Optimization

Stefan Boettcher*, Physics Department, Emory University, Atlanta, Georgia 30322, USA

September 23, 2024

Abstract

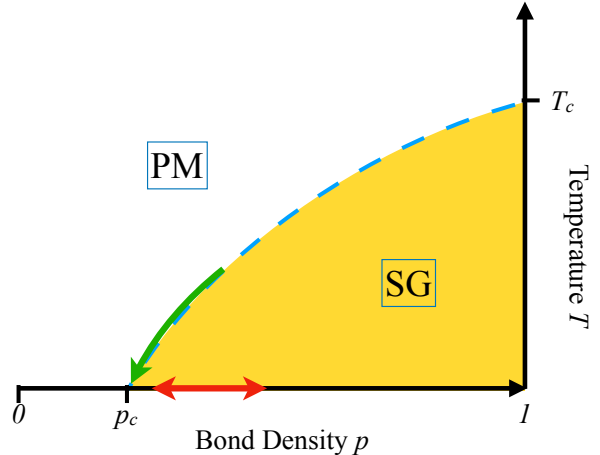
We present a collection of simulations of the Edwards-Anderson lattice spin glass at $T = 0$ to elucidate the nature of low-energy excitations over a range of dimensions that reach from physically realizable systems to the mean-field limit. Using heuristic methods, we sample ground states of instances to determine their energies while eliciting excitations through manipulating boundary conditions. We exploit the universality of the phase diagram of bond-diluted lattices to make such a study in higher dimensions computationally feasible. As a result, we obtain a verity of accurate exponents for domain wall stiffness and finite-size corrections that allow us to examine their dimensional behavior and their connection with predictions from mean-field theory. We also provide an experimentally testable prediction for the thermal-to-percolative crossover exponent in dilute lattices Ising spin glasses.

1 Introduction

Imagining physical systems in non-integer dimensions, such as through the ϵ -expansion [1] or *dimensional regulation* [2], to name but two, has provided many important results for the understanding of the physics in realistic dimensions. For example, the goal of the ϵ -expansion is to establish a connection between the (technically, infinite-dimensional) mean-field solution of a field theory and its real-space behavior. For a disordered system such as a spin glass [3–6], this playbook has proved rather difficult to follow theoretically [7–9]. In contrast, we endeavor to explore the transition between the often well-known mean-field properties and their modifications in real space using numerical means, free of any theoretical preconceptions. In this task, on top of the computational extensive disorder averages, the complexity of spin glasses reveals itself through increasingly slower convergence in thermal simulations, the deeper one pushes into the glassy regime. Going all the way to $T = 0$, then, makes thermal explorations impossible and renders the problem of finding the ground states NP-hard in general [10], in fact. However, simulations at $T = 0$ also avail us considerable conceptual clarity and an entirely new suit of techniques, albeit for just a few, yet important, observables. Some equilibrium properties of spin glasses below T_c can be obtained from merely determining ground state energies, such as domain wall stiffness, finite-size corrections, and thermal-percolative crossover exponents. To keep systematic errors low while also creating enough statistics for the disorder average, we need to employ fast but ultimately inexact heuristic methods to overcome NP-hardness. To reach a sensible scaling regime in system sizes N , especially in higher dimensions, also requires clever exploitation of the phase diagram of a spin glass. Here, we discuss together the results obtained from large-scale simulations conducted over several years and spread over a number of articles [11–15].

*<http://www.physics.emory.edu/faculty/boettcher>

Figure 1: Phase diagram for bond-diluted spin glasses ($d > d_l$). The entire spin-glass phase (SG) for $T < T_c$ and $p > p_c$ has a universal positive domain-wall exponent, $y > 0$. In our measurements, we therefore utilize an interval of bond densities at $T = 0$ (red arrow) where p is sufficiently above the scaling window near p_c (at finite system size) but small enough to asymptotically reach significant system sizes L . At $p = p_c$ and $T = T_c = 0$, we define the domain-wall exponent for a spin glass on the percolating cluster as $y = y_p (< 0)$. It allows to extract the thermal-percolative crossover exponent ϕ that describes the behavior along the boundary $T_c(p) \sim (p - p_c)^\phi$ for $p \searrow p_c$ (green arrow). In the paramagnetic phase (PM) for $p < p_c$ or $T > T_c$, defect energies due to domain walls decay exponentially.



To be specific, we simulate the Ising spin glass model due to Edwards and Anderson (EA) with the Hamiltonian [16]

$$H = - \sum_{\langle i,j \rangle} J_{i,j} \sigma_i \sigma_j. \quad (1)$$

The dynamic variables are binary (Ising) spins $\sigma_i = \pm 1$ placed on a hyper-cubic lattice in integer d dimension with couplings between nearest neighbors $\langle i, j \rangle$ via random bonds J_{ij} drawn from some distribution $\mathcal{P}(J)$ of zero mean and unit variance. The lattices are periodic with base length L in all directions, i.e., each such instance has $N = L^d$ spins. To relate real-world behavior in $d = 3$ (which is explored experimentally and theoretically in other articles in this collection) with mean-field behavior, which manifests itself above the upper critical dimension $d_u = 6$ [3], we find ground states of EA on lattices in $d = 3, \dots, 8$. In each d , we need to simulate instances over a wide range of L to be able to extrapolate our results to the thermodynamic limit ($L \rightarrow \infty$). At each size L , we further need to measure a large number of instances with independently drawn random bonds for the disorder average inherent to obtain observables in spin glasses. Each instance entails approximating its ground state, which is an NP-hard combinatorial problem.

To sample ground state energies at high through-put and with minimal systematic error, heuristics can only be relied on for systems with not too much more than $N \approx 1000$ spins coupled together. This would appear to limit the “dynamic range” in size up to around $L = 10$ in $d = 3$, but limited to $L = 6$ in $d = 4$ and even to $L < 3$ in $d = 7$, definitely insufficient to extract any $L \rightarrow \infty$ limit! However, the phase diagram for a bond-diluted EA system (with $d \geq 3$ such that $T_c > 0$) in Fig. 1 suggests that universal scaling behavior extends across the entire spin-glass phase (SG) down to the scaling window near the bond-percolation threshold p_c for low enough T , i.e., most definitely for $T = 0$. Thus, our strategy is to find ground states for EA instances at bond-density p with sufficient dynamic range in L for $p > p_c$ just above that scaling window to be within SG, using *exact* reduction methods [12, 17] (see Appendix A) to remove a large number of spins followed by heuristic optimization of remainder systems with $N_r \leq 1000$ [18, 19] (see Appendix B). These reduction methods recursively trace out all spins with fewer than four connected neighbors, at least, and are particularly effective near p_c , since each spin in EA has at most $2d$ potential neighbors while $p_c \sim 1/(2d)$ in large d such that for p just above p_c lattices remain sparse, each spin being connected to barely more than one other spin, on average, albeit with large variations. E.g., in $d = 8$ for $p = 0.0735 > p_c \approx 0.068$ and $L = 6$, an EA system with $N = 6^8 \approx 1.7 \times 10^6$ spins typically reduces to

a remainder graph with $\langle N_r \rangle \approx 1000$ spins, each connected to 5.3 neighbors, on average, to be optimized heuristically.

2 Domain Wall Stiffness Exponents

A quantity of fundamental importance for the modeling of amorphous magnetic materials through spin glasses [3, 20–23] is the domain-wall or “stiffness” exponent y , often also labeled θ . As Hook’s law describes the response to increasing elastic energy imparted to a system for increasing displacement L from its equilibrium position, the stiffness of a spin configuration describes the typical rise in magnetic energy ΔE due to an induced defect-interface of a domain of size L . But unlike uniform systems with a convex potential energy function over its configuration space (say, a parabola for the single degree of freedom in Hook’s law, or a high-dimensional funnel for an Ising ferromagnet), an amorphous many-body system exhibits a function more reminiscent of a high-dimensional mountain landscape. Any defect-induced displacement of size L in such a complicated energy landscape may move a system through numerous undulations in energy ΔE . Averaging over many incarnations of such a system results in a typical energy scale

$$\sigma(\Delta E) \sim L^y \quad (L \rightarrow \infty) \quad (2)$$

for the standard deviations of the domain wall energy ΔE .

The importance of this exponent for small excitations in disordered spin systems has been discussed in many contexts [22, 24–28]. Spin systems with $y > 0$ provide resistance (“stiffness”) against the spontaneous formation of defects at sufficiently low temperatures T ; an indication that a phase transition $T_c > 0$ to an ordered state exists. For instance, in an Ising ferromagnet, the energy ΔE is always proportional to the size of the interface, i. e. $y = d - 1$, consistent with the fact that $T_c > 0$ only when $d > 1$. For $y < 0$, the state of a system is unstable with respect to defects, and spontaneous fluctuations may proliferate, preventing any ordered state. Thus, determining the exact “lower critical dimension” d_l , where $y|_{d=d_l} = 0$, is of singular importance, and understanding the mechanism leading to d_l , however un-natural its value, provides clues to the origin of order [13, 29–33].

Instead of waiting for a thermal fluctuation to spontaneously induce a domain-wall, it is expedient to directly impose domains of size L through reversed boundary conditions on the system and measure the energy needed to determine y . To wit, in a system with periodic boundary conditions, we first obtain its ground state E_0 unaltered and obtain it again as E'_0 after reversing the signs on all bonds within a $(d - 1)$ -dimensional hyperplane, resulting in a complex domain of spins of size $\sim L$ that are reversed between both ground states such that $\Delta E = E_0 - E'_0$ is the energy due to the interface of that domain. Since ΔE is equally likely to be positive or negative, it is its deviation, $\sigma(\Delta E)$, which sets the energy scale in Eq. (2). Note that this problem puts an even higher demand on the ground state heuristic than described in the introduction. Here, the domain-wall energy ΔE is a minute, sub-extensive difference between two almost identical, extensive energies, E_0 and E'_0 , each of which is NP-hard to find. Thus, any systematic error would escalate rapidly with N_r , the size of the remainder graph.

As shown in Fig. 2, using bond-diluted lattices for EA, in contrast, not only affords us a larger dynamic range in L , but also allows for an extended scaling regime due to the additional parameter of p ranging over an entire interval. Instead of one set of data for increasing L at a fixed p (typically, $p = 1$ [34]) leading to the scaling in Eq. (2), we can scale multiple independent sets for such a range of p into a collective scaling variable, $\mathcal{L} = L(p - p^*)^y$, that collapses the data according to $\sigma(L, p) \sim \mathcal{L}^y$. While the extension to an interval in p makes simulations more laborious, it typically yields an extra order of magnitude in scaling compared to the prohibitive effort of confronting the NP-hard problem of reaching large L at fixed p alone. For instance, in $d = 3$ at $p = 1$, attainable sizes span $3 \leq L \leq 12$, at best, while we obtain a perfect data

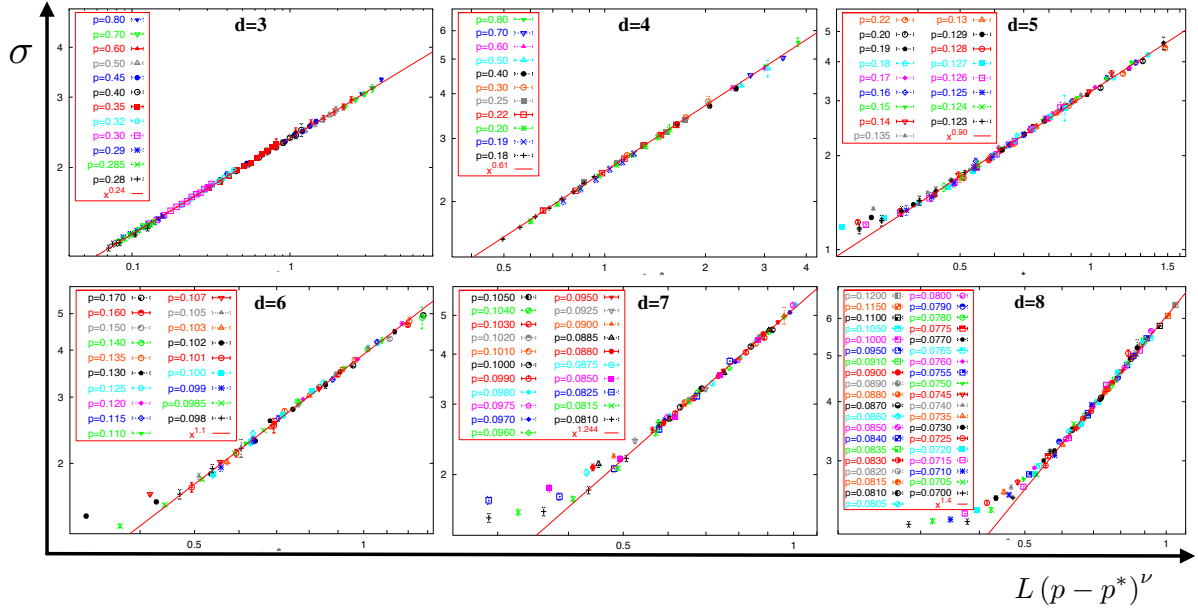


Figure 2: Data collapse for the domain wall scaling simulations of bond-diluted EA in $d = 3, \dots, 8$ of $\sigma(L, p) \sim \mathcal{L}^y$ in the scaling variable $\mathcal{L} = L(p - p^*)^\nu$. For each d , data sets are created over a range in p as listed in the respective legend, up to a size L such that remainder graphs are typically $< \langle N_r \rangle \approx 10^3$. The original data and the fitting parameters are listed in Refs. [11, 12]. The obtained domain wall scaling exponents y_d are listed in Tab. 1. Note that for $d \leq 4$, transient data for smaller \mathcal{L} has been omitted for clarity.

collapse for about $0.07 \leq \mathcal{L} \leq 3$ for $0.28 \leq p \leq 0.8$. (Note that while $p^* \approx p_c$ and ν has some relation to the correlation-length exponent in percolation, see below, it is necessary to allow these to be a free parameter for the bimodal bonds used in these simulations, as was argued in Ref. [12].) The fitted values for y for each d , as obtained from Fig. 2, are listed in Tab. 1.

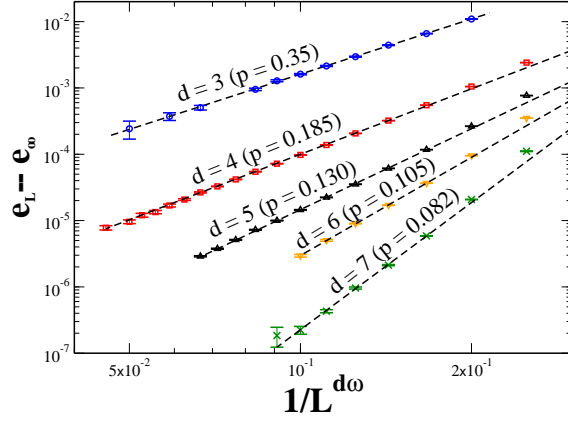
These values for y are listed in Tab. 1 and plotted in Fig. 4 as $1 - \frac{y}{d}$. That quantity has been obtained in the mean-field case by Parisi and Rizzo [35], yielding $1 - \frac{y}{d} = \frac{5}{6}$ above the upper critical dimension, $d \geq d_u = 6$. That value is clearly consistent with our high-dimensional data, providing a rare direct comparison between the mean field theory (RSB) and real-world spin glasses. As Fig. 4 further shows, the exponent varies continuously with dimension d and allows for a simple cubic fit of the numerical data between $2 \leq d \leq 6$, weighted by the statistical errors [13]. The fit *independently* reproduces the exactly-known result *outside* the fitted domain at $d = 1$, $y = -1$, to less than 0.8% (not shown here). The fit has a zero at $d_l \approx 2.498$ and yields $y \approx 0.001$ at $d = \frac{5}{2}$; strong evidence that $d_l = 5/2$, which has been suggested also by theory [30, 33] and is consistent with experiment [32].

In the following, we will consider some other uses of the domain-wall excitations.

3 Ground State Finite-Size Correction Exponents

Since simulations of statistical systems are bound to be conducted at system sizes N typically quite far from the thermodynamic limit $N \rightarrow \infty$, it becomes essential to understand the corrections entailed by such limitation. This is especially pertinent for spin glasses beset with extra complexities such as NP-hardness at $T = 0$ (or, similarly, the lack of equilibration at low but finite T) or the additional burden of disorder averaging over many random samples severely limiting N . Only rarely do such corrections decay fast

Figure 3: Plot of finite-size corrections to ground state energies in bond-diluted lattice spin glasses (EA). For each dimension d , ground state averages e_L at increasing system sizes L were obtained at a convenient bond-density p . An asymptotic fit (dashed lines) of that data according to Eq. (3) was obtained. The resulting values for the finite-size corrections exponent ω are listed in Tab. 1 and plotted in Fig. 4, suggesting that Eq. (4) holds.



enough to reveal the thermodynamic behavior of an observable in a simulation at a single, “large-enough” N . Instead, as we have already seen for the stiffness in Sec. 2, typically, sets of data need to be generated to glean the asymptotic behavior for large sizes. To extrapolate for the value of an intensive observable (like the ground-state energy density) it is then necessary to have a handle on the nature of the finite-size corrections (FSC) that have to be expected for the generated data [25, 40, 41]. However, FSC are not only a technical necessity. Their behavior is often closely related to other physical properties in the thermodynamic limit via scaling relations [27]. They can also be instrumentalized, for instance, to assess the scaleability of optimization heuristics [42, 43].

For the ground state energy densities in EA, Ref. [27] argued that such FSC should be due to locked-in domain walls of energy $\sim L^y$, which would lead to the scaling correction for the extensive energies of $E_L \sim e_\infty L^d + \Upsilon L^y$ for large L , defining e_∞ as the $L \rightarrow \infty$ limit of the average ground state energy density $e_L = \langle \frac{E_L}{L^d} \rangle$. This is consistent with Eq. (2), where we have purposefully created such a domain wall, because the same system freed from that domain wall (or locked into another one) would have $E_L^f \sim e_\infty L^d + \Upsilon' L^y$,

Table 1: Stiffness exponents for Edwards-Anderson spin glasses [11, 12] for dimensions $d = 2, \dots, 8$ obtained numerically from domain-wall excitations of ground states, as in Fig. 2. The next column contains the measured values for finite-size corrections, denoted as ω , from the fit of the data in Fig. 3. The stiffness exponents y_P obtained in Ref. [14] refer to EA at the bond-percolation threshold p_c , with values of p_c taken from Ref. [36] for $d = 3$ and Ref. [37] for $d \geq 4$. The correlation-length exponents ν for percolation are from Ref. [38] in $d = 3$ and from Ref. [39] for $d \geq 4$, where $\nu = 1/2$ is exact above the upper critical dimension, $d \geq 6$.

d	y	$1 - y/d$	ω	y_P	$1 - y_P/d$	p_c	ν	$\phi = -\nu y_P$
2	-0	1.141(1)		-0	1.497(2)	$\frac{1}{2}$	$\frac{4}{3}$	1.323(4)
3	0	0.920(4)	0	-1	1.429(3)	0	0.87436(46)	1.127(5)
4	0	0.847(3)	0	-1	1.393(2)	0	0.70(3)	1.1(1)
5	0	0.824(10)	0	-1	1.37(1)	0	0.571(3)	1.05(2)
6	1	0.82(2)	0	-2	1.34(1)	0	$\frac{1}{2}$	1.00(2)
7	1	0.823(7)	0	-2	1.33(1)	0	$\frac{1}{2}$	1.14(3)
8	1	0.85(2)						
∞	$\sim \frac{d}{6}$	$\frac{5}{6} = 0.8333$			$\frac{4}{3} = 1.333$	$\sim \frac{1}{2d}$	$\frac{1}{2}$	$\sim \frac{d}{6} (?)$

thus, $\Delta E_L \sim \Delta Y L^y$. Dividing E_L by system size, we then get

$$e_L \sim e_\infty + \frac{A}{(L^d)^\omega}, \quad (L \rightarrow \infty). \quad (3)$$

where the FSC exponent is conjectured to be

$$\omega = 1 - \frac{y}{d}. \quad (4)$$

Indeed, our direct evaluation of ground state energy densities at some fixed bond density p in dimensions $d = 3, \dots, 7$ shown in Fig. 3 are convincingly in agreement with this picture for the dominant contributions to FSC. However, that leaves us with somewhat of a conundrum when compared with mean-field simulations, where FSC for the Sherrington-Kirkpatrick spin glass model (SK) [44–46] appear to yield $\omega \approx \frac{2}{3}$ for $d \rightarrow \infty$, which is not close to $1 - y/d \rightarrow \frac{5}{6}$ from RSB theory [35].

We conducted a corresponding ground state study at the edge of the SG regime (see Fig. 1) by choosing the percolation point $p = p_c$ exactly. Since the fractal percolation cluster cannot sustain an ordered state, we find that the stiffness exponent defined in Eq. (2) is negative there, $y|_{p=p_c} = y_p < 0$. Numerical studies of ground states at p_c (using Gaussian bonds J_{ij} in this case) is computationally quite efficient, since the fractals embedded in the lattice reduce often completely or so substantially that heuristics produce little systemic error. Large lattice sizes L can be achieved, limited only by rare large remainder graphs or the lack of memory needed to build the original, unreduced EA lattice. The values for y_p thus obtained [14] are also listed in Tab. 1. Although the hypothesis for FSC from Eq. (4), $\omega = 1 - y_p/d$, leads to large values for ω when $y_p < 0$ and it becomes hard to test numerically, the corrections found are well consistent with the hypothesis [15]. In particular, it appears that $1 - y_p/d \rightarrow \frac{4}{3}$ for $d \geq d_u = 6$, which would be consistent with FSC in percolating random graphs [47]. While this provides an argument that Eq. (4) should also hold in the mean-field limit for EA in the spin glass phase, SK might be a poor representation of that limit for EA. In EA, we first let $L \rightarrow \infty$ for fixed number of neighbors $2dp$ before $d \rightarrow \infty$, while in SK both system size and neighborhood diverge simultaneously. Unfortunately, also sparse mean-field spin glasses on regular graphs (“Bethe lattices”) appear to have FSC with $\omega = \frac{2}{3}$ [48], but those results might depend to some extent on structural details of the mean-field networks [45, 49, 50] and which structure most closely resembles a mean-field version of EA at $d \rightarrow \infty$ remains unclear.

4 Thermal-Percolative Crossover Exponents

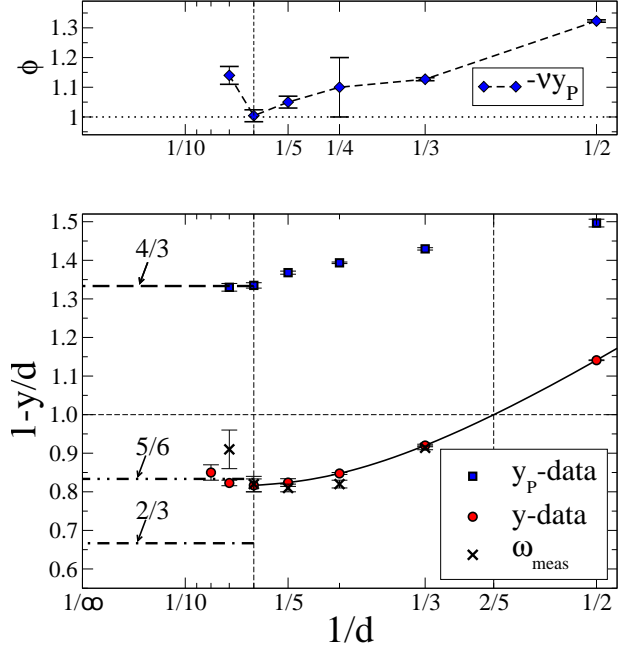
Having determined the percolative stiffness exponents y_p already in the previous section, we can utilize it to make an interesting – and potentially experimentally testable – prediction about the behavior of the phase transition line in Fig. 1. For diluted lattices at *variable* bond density $p \rightarrow p_c$, Eq. (2) generalizes to [51, 52]

$$\sigma(\Delta E)_{L,p} \sim \mathcal{Y}(p) L^y f(L/\xi(p)). \quad (5)$$

Here, we assume $\mathcal{Y}(p) \sim (p - p_c)^t \sim \xi^{-t/\nu}$ for the surface tension and $\xi(p) \sim (p - p_c)^{-\nu}$ is the conventional correlation length for percolation. The scaling function f is defined to be constant for $L \gg \xi(p) \gg 1$, where percolation (and hence, ξ) plays no role and we regain Eq. (2) for $p > p_c$. For $\xi \gg L \gg 1$, Eq. (5) requires $f(x) \sim x^\mu$ for $x \rightarrow 0$ to satisfy $\sigma \rightarrow 0$ with some power of L , needed to cancel the ξ -dependence at $p = p_c$. Thus, $\mu = -t/\nu$, and we obtain $y_p = y + \mu = y - t/\nu$ to mark the L -dependence of σ at $p = p_c$, as before, which yields $t = \nu(y - y_p)$. Finally, at the cross-over $\xi \sim L$, where the range L of the excitations $\sigma(\Delta E)$ reaches the percolation length beyond which spin glass order ensues, Eq. (5) provides

$$\sigma(\Delta E)_{\xi(p),p} \sim (p - p_c)^t \xi(p)^y f(1) \sim (p - p_c)^{-\nu y_p}. \quad (6)$$

Figure 4: Plot summarizing the data for the exponents in Tab. 1, here plotted as a function of inverse dimension, $1/d$, to highlight the connection with the mean field limit for $d \geq d_u = 6$ (left vertical line). The bottom plot refers to the stiffness exponents y in the spin-glass regime (SG in Fig. 1) or y_P at p_c and $T = 0$, each presented as $1 - y/d$. Included are also the measured FSC exponents ω , which appear to be consistent with the conjecture in Eq. (4). For stiffness, the y -data is quite consistent with $1 - y/d = 5/6$ predicted for $d \geq d_u$ [35], but not with the FSC $\omega_{\text{SK}} = 2/3$ found for SK [44]. Fit of this data (solid line) yields a lower critical dimension $d_l \approx \frac{5}{2}$, where $y = 0$ (right vertical line). At p_c , the y_P -data appears to approach a value of $\omega = 4/3$ expected for FSC of percolating random graphs. In the top plot, y_P is multiplied with the independent percolation exponent ν to form the thermal-percolative crossover exponent ϕ that characterizes the behavior of the phase boundary near p_c in Eq. (7), see green arrow in Fig. 1. It seems to show a minimum of $\phi \approx 1$ at $d = d_u = 6$.



Associating a temperature with the energy scale of this cross-over by $\sigma(\Delta E)_{\xi(p),p} \sim T_c$ (since, for $T > T_c$, thermal fluctuations destroy order at a length-scale $\ll \xi$), leads to

$$T_g(p) \sim (p - p_c)^\phi, \quad \text{with } \phi = -\nu y_P, \quad (7)$$

defining [51] the “thermal-percolative cross-over exponent” ϕ . All data for $d = 2, \dots, 7$ are listed in Tab. 1, the results for ϕ are also shown in Fig. 4. It appears that ϕ declines with increasing d for $d \leq d_u = 6$, has a minimum of $\phi = 1$ at $d_u = 6$, and rises as $\phi = d/6$ above d_u .

Of particular experimental interest is the result for $d = 3$, $y_P = -1.289(6)$, predicting $\phi = 1.127(5)$ with $\nu = 0.87436(46)$. [38] This exponent provides a non-trivial, experimentally testable prediction derived from scaling arguments of the equilibrium theory at low temperatures. (Since bond and site percolation are typically in the same universality class, it should make little difference whether an experiment varies the site-concentration of atoms with dipolar spin or the bonds between them.) Such tests are few as disordered materials by their very nature fall out of equilibrium when entering the glassy state. The phase boundary itself provides the perfect object for such a study: It can be approached by theory from below and by experiments from above where equilibration is possible. Ref. [53] already provided highly accurate results for the freezing temperature T_M as a function of dilution x for a doped, crystalline glass, $(\text{La}_{1-x}\text{Gd}_x)_{80}\text{Au}_{20}$, proposing a linear dependence, $T_M \sim x$. The tabulated data is equally well fitted by Eq. (7) in that regime. Ref. [54] determined a phase diagram for $(\text{Fe}_x\text{Ni}_{1-x})_{75}\text{P}_{16}\text{B}_6\text{Al}_4$, an amorphous alloy, for a wide range of temperatures T and site-concentrations x but did not discuss its near-linear behavior at low x . A similar phase diagram for the insulator $\text{CdCr}_{2x}\text{In}_{2(1-x)}\text{S}_4$ can be found in Fig. 1.1a of Ref. [55]. New experiments dedicated to the limit $x \searrow x_c$ should provide results of sufficient accuracy to test our prediction for ϕ .

5 Conclusions

We have summarized a collection of simulation data pertaining to the lattice spin glass EA over a range of dimensions, providing a comprehensive description of low-energy excitations from experimentally accessible systems to the mean-field level, where exact results can be compared with. Putting all those results side-by-side paints a self-consistent picture of domain-wall excitations, their role in the stability of the ordered glass state, and their role for finite-size corrections. Extending to the very physical concept of bond-density made simulations in high dimensions feasible, added accuracy, and opened up the spin-glass phase diagram, which makes new observables experimentally accessible, such as the thermal-percolative crossover exponent.

Going forward, the methods developed here could be extended to study, say, ground state entropy and their overlaps [56] or the fractal nature of domain walls [57, 58]. Our method might inspire also new ways of using dilution as a gadget to make simulations more efficient [59].

References

- [1] K. G. Wilson and M. E. Fisher, *Phys. Rev. Lett.* **28**, 240 (1972).
- [2] G. 't Hooft and M. J. G. Veltman, *Nucl. Phys. B* **44**, 189 (1972).
- [3] K. H. Fischer and J. A. Hertz, *Spin Glasses*, Cambridge Studies in Magnetism (Cambridge University Press, Cambridge, 1991).
- [4] M. Mézard, G. Parisi, and M. A. Virasoro, *Spin glass theory and beyond* (World Scientific, Singapore, 1987).
- [5] D. L. Stein and C. M. Newman, *Spin Glasses and Complexity* (Princeton University Press, Princeton, 2013).
- [6] P. Charbonneau, E. Marinari, and M. Mezard, eds., *Spin glass theory and far beyond* (World Scientific, Singapore, 2023).
- [7] C. de Dominicis, I. Kondor, and T. Temesári, in *Spin Glasses and Random Fields*, edited by A. Young (World Scientific, Singapore, 1998).
- [8] M. A. Moore and N. Read, *Physical Review Letters* **120**, 130602 (2018).
- [9] M. A. Moore, *Physical Review E* **103**, 062111 (2021).
- [10] F. Barahona, *J. Phys. A: Math. Gen.* **15**, 3241 (1982).
- [11] S. Boettcher, *The European Physical Journal B - Condensed Matter* **38**, 83 (2004).
- [12] S. Boettcher, *Europhys. Lett.* **67**, 453 (2004).
- [13] S. Boettcher, *Physical Review Letters* **95**, 197205 (2005).
- [14] S. Boettcher and E. Marchetti, *Phys. Rev. B* **77**, 100405(R) (2008).
- [15] S. Boettcher and S. Falkner, *EPL (Europhysics Letters)* **98**, 47005 (2012).
- [16] S. F. Edwards and P. W. Anderson, *J. Phys. F* **5**, 965 (1975).
- [17] S. Boettcher and J. Davidheiser, *Phys. Rev. B* **77**, 214432 (2008).

- [18] S. Boettcher and A. G. Percus, *Physical Review Letters* **86**, 5211 (2001).
- [19] A. Hartmann and H. Rieger, eds., *New Optimization Algorithms in Physics* (Wiley-VCH, Berlin, 2004).
- [20] B. W. Southern and A. P. Young, *J. Phys. C: Solid State Phys.* **10**, 2179 (1977).
- [21] W. L. McMillan, *J. Phys. C: Solid State Phys.* **17**, 3179 (1984).
- [22] D. S. Fisher and D. A. Huse, *Phys. Rev. Lett.* **56**, 1601 (1986).
- [23] A. J. Bray and M. A. Moore, in *Heidelberg Colloquium on Glassy Dynamics and Optimization*, edited by L. Van Hemmen and I. Morgenstern (Springer, New York, 1986), p. 121.
- [24] F. Krzakala and O. Martin, *Phys. Rev. Lett.* **85**, 3013 (2000).
- [25] M. Palassini and A. P. Young, *Phys. Rev. Lett.* **85**, 3017 (2000).
- [26] M. Palassini, F. Liers, M. Juenger, and A. P. Young, *Physical Review B* **68**, 064413 (2003).
- [27] J.-P. Bouchaud, F. Krzakala, and O. C. Martin, *Phys. Rev. B* **68**, 224404 (2003).
- [28] T. Aspelmeier, M. A. Moore, and A. P. Young, *Phys. Rev. Lett.* **90**, 127202 (2003).
- [29] A. J. Bray and M. A. Moore, *J. Phys. C: Solid State Phys.* **17**, L463 (1984).
- [30] S. Franz, G. Parisi, and M. A. Virasoro, *J. Phys. I (France)* **4**, 1657 (1994).
- [31] A. K. Hartmann and A. P. Young, *Phys. Rev. B* **64**, 180404(R) (2001).
- [32] S. Guchhait and R. Orbach, *Phys. Rev. Lett.* **112**, 126401 (2014).
- [33] A. Maiorano and G. Parisi, *Proceedings of the National Academy of Sciences* **115**, 5129 (2018).
- [34] A. K. Hartmann, *Physical Review E* **63**, 016106 (2000).
- [35] G. Parisi and T. Rizzo, *Phys. Rev. Lett.* **101**, 117205 (2008).
- [36] C. D. Lorenz and R. M. Ziff, *Phys. Rev. E* **57**, 230 (1998).
- [37] P. Grassberger, *Phys. Rev. E* **67**, 036101 (2003).
- [38] Y. Deng and H. W. J. Blöte, *Phys. Rev. E* **72**, 016126 (2005).
- [39] B. D. Hughes, *Random Walks and Random Environments* (Oxford University Press, Oxford, 1996).
- [40] K. F. Pal, *Physica A* **233**, 60 (1996).
- [41] A. Young, *Finite-Size Scaling* (World Scientific, 2024), pp. 599–615.
- [42] S. Boettcher, *Physical Review Research* **1**, 033142 (2019).
- [43] S. Boettcher, *Nature Communications* **14**, 5658 (2023).
- [44] S. Boettcher, *The European Physical Journal B* **46**, 501 (2005).
- [45] S. Boettcher, *Journal of Statistical Mechanics: Theory and Experiment* **2010**, P07002 (2010).

- [46] T. Aspelmeier, A. Billoire, E. Marinari, and M. A. Moore, *Journal of Physics A: Mathematical and Theoretical* **41**, 324008 (2008).
- [47] B. Bollobas, *Random Graphs* (Academic Press, London, 1985).
- [48] S. Boettcher, *The European Physical Journal B - Condensed Matter* **31**, 29 (2003).
- [49] L. Zdeborová and S. Boettcher, *Journal of Statistical Mechanics: Theory and Experiment* **2010**, P02020 (2010).
- [50] S. Boettcher, *Physical Review Letters* **124**, 177202 (2020).
- [51] J. R. Banavar, A. J. Bray, and S. Feng, *Phys. Rev. Lett.* **58**, 1463 (1987).
- [52] A. J. Bray and S. Feng, *Phys. Rev. B* **36**, 8456 (1987).
- [53] S. J. Poon and J. Durand, *Phys. Rev. B* **18**, 6253 (1978).
- [54] O. Beckman, E. Figueroa, K. Gramm, L. Lundgren, K. V. Rao, and H. S. Chen, *Phys. Scr.* **25**, 726 (1982).
- [55] E. Vincent, in *Ageing and the Glass Transition*, edited by M. Henkel, M. Pleimling, and R. Sanctuary (Springer, Heidelberg, 2007), vol. 716 of *Springer Lecture Notes in Physics*, condmat/063583.
- [56] S. Boettcher, *The European Physical Journal B - Condensed Matter* **33**, 439 (2003).
- [57] W. Wang, M. A. Moore, and H. G. Katzgraber, *Physical Review Letters* **119** (2017).
- [58] B. Vedula, M. A. Moore, and A. Sharma, *Evidence that the at transition disappears below six dimensions* (2024).
- [59] T. Jörg and F. Ricci-Tersenghi, *Phys. Rev. Lett.* **100**, 177203 (2008).
- [60] S. Boettcher and A. Percus, *Artificial Intelligence* **119**, 275 (2000).
- [61] S. Boettcher and M. Grigni, *Journal of Physics A: Mathematical and General* **35**, 1109 (2002).
- [62] S. Boettcher and M. Paczuski, *Physical Review E* **54**, 1082 (1996).
- [63] S. Boettcher, in *Lecture Notes in Computer Science*, edited by T. Stützle (Springer Berlin Heidelberg, 2009), vol. 5851, pp. 1–14.

Supplementary Material

Appendix A: Bond-Diluted Spin Glasses

We have developed an exact algorithm that is capable of drastically reducing the size of sparsely connected spin glass systems [11], leaving a much reduced remainder graph whose ground state can be approximated with great accuracy using heuristics, such as EO. The algorithm and its efficiency is studied in more detail elsewhere [17]. An extension to simultaneously compute the entropy density and overlap for sparse spin glass systems is discussed in Ref. [56]). We focus here exclusively on the reduction rules for the energy at $T = 0$. These rules apply to general, purely quadratic Ising spin glass Hamiltonians such as Eq. (1). The reductions effect both spins and bonds, eliminating recursively all zero-, one-, two-, and three-connected spins. These operations eliminate and add terms to the expression in Eq. (1), but leave it form-invariant. Offsets in the energy along the way are accounted for by a variable H_o , which is *exact* for a ground state configuration.

Rule I: An isolated spin can be ignored entirely.

Rule II: A one-connected spin i can be eliminated, since its state can always be chosen in accordance with its neighboring spin j to satisfy the bond $J_{i,j}$. For its energetically most favorable state we adjust $H_o := H_o - |J_{i,j}|$ and eliminate the term $-J_{i,j} \sigma_i \sigma_j$ from H .

Rule III: A double bond, $J_{i,j}^{(1)}$ and $J_{i,j}^{(2)}$, between two vertices i and j can be combined to a single bond by setting $J_{i,j} = J_{i,j}^{(1)} + J_{i,j}^{(2)}$ or be eliminated entirely, if the resulting bond vanishes. This operation is very useful to lower the connectivity of i and j by one.

Rule IV: Replacing a two-connected spin i between some spins 1 and 2, the graph obtains a new bond $J_{1,2}$, and acquires an offset $H_o := H_o - \Delta H$, by rewriting in Eq. (1)

$$\begin{aligned} \sigma_i(J_{i,1}\sigma_1 + J_{i,2}\sigma_2) &\leq |J_{i,1}\sigma_1 + J_{i,2}\sigma_2| = J_{1,2}\sigma_1\sigma_2 + \Delta H, \\ J_{1,2} &= \frac{1}{2}(|J_{i,1} + J_{i,2}| - |J_{i,1} - J_{i,2}|), \quad \Delta H = \frac{1}{2}(|J_{i,1} + J_{i,2}| + |J_{i,1} - J_{i,2}|). \end{aligned} \quad (8)$$

Rule V: A three-connected spin i can be reduced via a “star-triangle” relation, see Fig. ??:

$$\begin{aligned} J_{i,1}\sigma_i\sigma_1 + J_{i,2}\sigma_i\sigma_2 + J_{i,3}\sigma_i\sigma_3 &\leq J_{1,2}\sigma_1\sigma_2 + J_{1,3}\sigma_1\sigma_3 + J_{2,3}\sigma_2\sigma_3 + \Delta H, \\ J_{1,2} &= -A - B + C + D, \quad J_{1,3} = A - B + C - D, \quad J_{2,3} = -A + B + C - D, \\ \Delta H &= A + B + C + D, \quad A = \frac{1}{4}|J_{i,1} - J_{i,2} + J_{i,3}|, \\ B &= \frac{1}{4}|J_{i,1} - J_{i,2} - J_{i,3}|, \quad C = \frac{1}{4}|J_{i,1} + J_{i,2} + J_{i,3}|, \quad D = \frac{1}{4}|J_{i,1} + J_{i,2} - J_{i,3}|. \end{aligned} \quad (9)$$

Rule VI: A spin i (of any connectivity) for which the absolute weight $|J_{i,j'}|$ of one bond to a spin j' is larger than the absolute sum of all its other bond-weights to neighboring spins $j \neq j'$, i. e., it’s a “super-bond” with

$$|J_{i,j'}| > \sum_{j \neq j'} |J_{i,j}| \quad (10)$$

such that bond $J_{i,j'}$ *must* be satisfied in any ground state. Then, spin i is determined in the ground state by spin j' and it as well as the bond $J_{i,j'}$ can be eliminated accordingly. Here, we obtain $H_o := H_o - |J_{i,j'}|$. All other bonds connected to i are simply reconnected with j' , but with reversed sign, if $J_{i,j'} < 0$.

This procedure is costly, and hence best applied after the other rules are exhausted. But it can be highly effective for widely distributed bonds, e.g., for Gaussian rather than bimodal $\mathcal{P}(J)$. In particular, since neighboring spins may reduce in connectivity and become susceptible to the previous rules again, an avalanche of further reductions may ensue.

The bounds in Eqs. (8-9) become *exact* when the remaining graph takes on its ground state. Reducing higher-connected spins leads to (hyper-)bonds between multiple spins, unlike Eq. (1), and is not considered here.

After a recursive application of these rules, the original lattice graph is either completely reduced (which is almost always the case for bond densities $p < p_c$), in which case H_o provides the exact ground state energy already, or we are left with a highly reduced, compact graph in which no spin has less than four connections. We obtain the ground state of the reduced graph with EO, which together with H_o provides a very accurate approximation to the ground state energy of the original diluted lattice instance.

Appendix B: Extremal Optimization Heuristic

For all of the results presented in this work, we have employed the Extremal Optimization heuristic (EO), specifically τ -EO [18, 19, 60], that performs a local search on an existing configuration $\vec{\sigma}$ by changing preferentially those σ_i of “bad” fitness λ_i . Here, the fitness for each spin σ_i is defined as the ratio of the sum of its satisfied weights over all its bond-weights, $\lambda_i = \sum_j^{\text{SAT}} |J_{i,j}| / \sum_j |J_{i,j}|$, so that $0 \leq \lambda_i \leq 1$. EO *ranks* variables by fitnesses, $\lambda_{\Pi(1)} \leq \lambda_{\Pi(2)} \leq \dots \leq \lambda_{\Pi(N)}$, where the permutation $\Pi(k) = i$ is the index for the k^{th} -ranked σ_i , then randomly selects a rank with a *scale-free* probability $P_k \propto k^{-\tau}$. The selected variable $\sigma_{\Pi(k)}$ is updated *unconditionally*, and it and all its neighbors reevaluate and rerank their λ_i . For an easily determined choice [18, 60] of τ (for which theory [19, 61] predicts as optimal choice $\tau_{\text{opt}} - 1 \sim \ln^{-1} N$), these unconditional updates ensure a build-up of large, highly correlated fluctuations through “adaptive avalanches” that *learn* and *memorize* (as expressed within that ranking) what is favored in an optimal solutions [62, 63]. It is the persistent bias against badly-adapted variables that leads to frequent returns to near-optimal configurations. As τ -EO keeps fluctuating widely, it simply records the best-found solution for the ground-state energy in passing, making it ideally suited also to time-varying problems as well as annealing operations, unencumbered by phase transitions [42].